Target Detection in Sea-Clutter Using Stationary Wavelet Transforms

Vichet Duk
University of Adelaide
AUSTRALIA
vichet.duk@adelaide.edu.au

Luke Rosenberg
Defence Science and Technology Group
AUSTRALIA
luke.rosenberg@dsto.defence.gov.au

Brian Ng
University of Adelaide
AUSTRALIA
brian.ng@adelaide.edu.au

ABSTRACT

Small target detection in the maritime environment remains a challenging problem. Maritime radars traditionally use non-coherent processing methods due to the time-varying and range-varying nature of the Doppler spectra. However, the radar backscatter may contain sea-spikes which can last for seconds and resemble targets. This paper presents an application of stationary wavelet transforms (SWT) to improve target detection in medium grazing angle X-band sea-clutter. Since different components (sub-bands) of the SWT decomposition reveal different spectral characteristics of the returned signal, a method of selecting the appropriate sub-band is presented using an entropy based metric. A Monte Carlo simulation using a cell averaging constant false alarm rate detector is then used to demonstrate the improvement of the SWT scheme against unfiltered data.

1.0 INTRODUCTION

The need to detect small targets on the sea surface from high flying platforms has increased the interest in alternate detection methods for airborne surveillance radars. When operating at higher grazing angles, the clutter return increases in intensity and reduces the performance that can be achieved by traditional non-coherent methods. In addition, the radar backscatter will contain sea-spikes which can last for seconds and cause false detections [1–3]. To minimise these and improve the detection performance, one potential solution is through the use of time-frequency representations. In this paper, a method of time-frequency signal processing, namely the stationary wavelet transform is explored.

There have been a number of studies into the use of wavelet transforms (WT) for detecting targets in sea-clutter. Ehara *et al.* [4] proposed two methods to improve the signal to noise ratio (SNR) of the radar echo return. The first is based on the idea that given an optimal scale, the wavelet function can approximate a matched filter and therefore improve target detection. The second method extends this idea by integrating a small range of wavelet coefficients around the optimal scale. This method provides more robustness and was shown to improve the SNR even further. Wang *et al.* [5] then proposed the use of a wavelet based function to replace the waveform in a radar system. If the returned signal was then matched to the wavelet function, it should appear stronger in the discrete wavelet transform (DWT) domain while the noise will be small and spread out. By suppressing these noise values with a threshold (de-noising), the SNR of the returned signal should then substantially increase. However, it was found that matching the wavelet waveform was difficult unless the target was large and had sufficient radar cross section (RCS). Zhang *et al.* [6] also used WTs for radar target detection and found that removing some of the high frequency ‘detail’ wavelet coefficients was effective in reducing the noise of radar echoes and thus improving detection performance. With this approach, the DWT sub-bands suffer from reduced detail (resolution), so the authors applied an independent component

analysis to the wavelet coefficients to improve the performance. However, with a single simulation and limited experimental details, it is unclear whether this approach is effective for a broader range of signals. Another wavelet-based approach was proposed by Davidson *et al.* [7], who used a continuous wavelet transform (CWT) to identify the dominant scatterers in a given scenario. The authors then applied a 'persistence' statistic to detect slow-moving targets from the surrounding backscatter.

In contrast to these existing wavelet-based schemes, we have investigated the use of two dimensional (2D) SWTs [8]. In this work, a single level 2D SWT was applied to the range / time domain with the filtered outputs individually reconstructed to produce four different range-time images. Analysis of the amplitude distribution of these reconstructed sub-bands revealed that some were less spiky than others and offered potential for improved detection performance. This was confirmed for both stationary and moving targets with Monte Carlo simulations using a cell averaging constant false alarm rate (CA-CFAR) detection scheme. Compared to unfiltered data, a good improvement was shown for moving targets while a slight improvement was found for stationary targets. A limitation of this work was the lack of a method to select which sub-band to use when the target velocity is unknown. In this paper, we now show that similar or better performance can be achieved with a one dimensional (1D) SWT applied along slow-time and by exploiting other decomposition levels of the SWT. Furthermore, we introduce a method of selecting the best decomposition structure, independent of the target velocity.

For this work, the Ingara X-band medium grazing angle sea-clutter data set has been used and is described in Section 2. A brief background to the SWT, its multi-resolution properties and details of the sub-band isolation is then given in Section 3. To gauge the possible detection performance of each reconstructed sub-band and combination, Section 4 looks at the mean separation between the interference (clutter + noise) and the target plus interference when a false target is injected into the data. However this approach is not practical in a real radar system where there is no prior knowledge of the target. To address this problem, an entropy based metric is introduced to indicate which reconstructed sub-band should offer the best detection performance [9–11]. The improvement in the detection performance of the complete algorithm when compared to unfiltered data is then given in Section 5.

2.0 Ingara sea-clutter data set

The Ingara medium grazing angle sea clutter data set was collected by the Defence Science and Technology Group (DST Group) in 2004 and 2006 [12]. The fully polarmetric X-band radar had a pulse repetition frequency (PRF) of 575 Hz and used a 200 MHz bandwidth giving 0.75 m range resolution. At a slant range of 3.4 km and with a 1° two-way 3dB azimuth beamwidth, the azimuth resolution was approximately 60 m. During the trial, radar backscatter was collected over 360° of azimuth and between $15^\circ - 45^\circ$ in grazing. For the comparisons in this paper, the dual polarised data set has been chosen from the 2006 trial with a Douglas sea state between 4 and 5. It comprises two subsequent runs where the radar first transmitted with a horizontal (H) polarisation and then with a vertical (V). Both runs received both H and V simultaneously. For the initial analysis, a 0.22 s data block has been chosen from the upwind direction covering 430 m with grazing angles between $30.5^\circ - 35.5^\circ$.

3.0 Wavelet transforms

Wavelet transforms have been used for signal processing in various applications to obtain compact representations of non-stationary signals. They have the ability to represent signals at multiple scales, or *resolutions*, with an adaptive time window, thus offering a different partitioning of the time frequency plane compared to techniques such as short time Fourier Transforms [13, 14]. The analysing functions in WT are dilated (by factor

a) and shifted (in time by b) versions of the same wavelet function $\psi(t)$,

$$\psi_{a,b}(t) = \frac{1}{\sqrt{a}}\psi\left(\frac{t-b}{a}\right). \tag{1}$$

A valid wavelet function must have a bandpass spectrum (zero average), and is thus a set of oscillations over a limited duration in the time domain.

3.1 Stationary wavelet transform

Multi-resoluton analysis separates non-stationary sea-clutter data into different sets of detail (projections onto wavelet functions, $\psi_{a,b}(t)$) and approximation (scaling function) coefficients, called *sub-bands*. Each of these coefficients corresponds to a unique region of the time-frequency plane. It is reasonable to expect interference and target returns would produce different distributions of coefficients, thus allowing them to be separated in the coefficient domain. In this work, we are using the SWT for its translation-invariance property [15, 16]. This is a non-decimated transform, and has been used successfully in applications which may be sensitive to artefacts that arise from the more popular, decimated version of the wavelet transform [15, 17].

The SWT signal decomposition algorithm is commonly implemented as cascaded two-channel filter banks, with each filter bank consisting of a pair of complementary low-pass and high-pass filters. The filter bank at level $k \geq 0$ accepts the approximation sub-band at level $k-1$ as an input and produces detail (D_k) and approximation (A_k) sub-bands at the outputs of the high- and low-pass filters, respectively. The data input is equivalent to the A_0 sub-band, with subsequent levels:

$$A_k(n) = \sum_{m\epsilon\mathcal{Z}} h_a(n-m)A_{k-1}(m), \tag{2}$$

$$D_k(n) = \sum_{m\epsilon\mathcal{Z}} g_a(n-m)A_{k-1}(m), \tag{3}$$

where $h_a(n)$ and $g_a(n)$ are the impulse responses of the low- and high-pass filters. The process can be reversed to perform reconstruction by

$$A_k(n) = \sum_{m\epsilon\mathcal{Z}} h_s(n-m)A_{k+1}(m) + \sum_{m\epsilon\mathcal{Z}} g_s(n-m)D_{k+1}(m) \tag{4}$$

where h_s and g_s are the low- and high-pass synthesis filters, respectively.

The set of filters $\{h_a, g_a, h_s, g_s\}$ must be designed together to achieve perfect (error-free) reconstruction. The literature describes numerous sets of wavelet filters, each designed to satisfy different properties [18]. A comprehensive survey of the performance of different wavelets is beyond the scope of this paper. Instead, we choose the popular Daubechies-4 wavelet for the analysis of the radar backscatter, based on earlier work [5].

3.2 Sub-band isolation

The SWT decomposition performed on the data leads to a number of different sub-bands. The components of the interference and target (if present) generally have different distributions of SWT coefficients across sub-bands. This implies that one or more sub-bands have a stronger signal to interference ratio (SIR) than the original data. It is based on this observation that we propose the use of a subset of SWT sub-bands for target detection. In order to combine the information from this subset, we perform a reconstruction back to the original time domain, choosing to retain only those selected sub-bands. This is equivalent to using zero inputs for the rejected sub-bands in the reconstruction algorithm. The *sub-band isolation and reconstruction* procedure is illustrated in Fig. 1. In the frequency domain, this can be interpreted as general band-pass filtering

with one or more pass-bands. The reconstruction from the level-1 approximate sub-band, $\tilde{A}_1$, only retains the low frequency part of the spectrum, while the reconstruction from the detail sub-band, $\tilde{D}_1$, only contains the high frequency part of the spectrum.

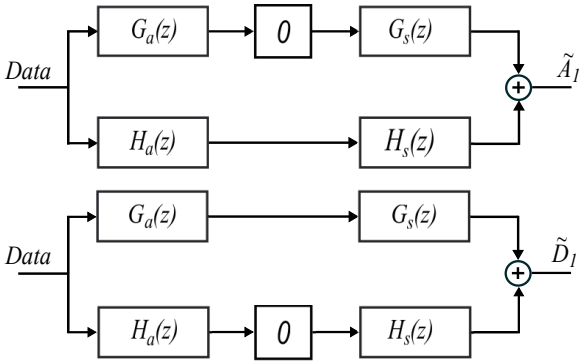

Figure 1: Data decomposition with sub-band isolation and reconstruction using 1D SWT: $\tilde{A}_1$ and $\tilde{D}_1$ are the approximate and detail reconstructed sub-bands of the original data.

In computing the SWT, the total number of levels is usually a user-chosen parameter. In our case, the finite number of pulses places a practical ceiling on the value of k. In the SWT decomposition, the filter impulse responses are up-sampled by 2 at every level of decomposition. This causes rapid growth in the length of these filters as the level increases, eventually reaching the length of the data series. Further decomposition beyond this ceases to produce meaningful sub-bands. More precisely, if there are M samples in slow-time, and the length of the analysis filters (h_a, g_a) is N, then the maximum level K must satisfy

$$K < \log_2\left(\frac{M}{N}\right). \tag{5}$$

For example, using length 8 Daubechies-4 filters for a coherent processing interval (CPI) of 128 pulses implies the SWT is limited to 4 levels or lower. However, for our analysis in this paper, we only use 3 levels to demonstrate the SWT performance. This simplifies the analysis and reduces the computational burden.

4.0 Sub-band analysis

Each reconstructed sub-band after the isolation is now analysed to investigate the impact of SWT on targets. Simulated non-fluctuating (Swerling 0) point targets with an SIR of 10 dB are injected into the HH polarised data. Figure 2 shows the 3-level decomposition of the data with two injected point targets (stationary and moving) at relative ranges of 190 m and 175 m respectively. The stationary target is always maintained in the reconstructed approximate sub-bands, $\tilde{A}_k$, and appears brighter at lower resolutions. The moving target has a higher Doppler frequency and is maintained in the reconstructed detail sub-band, $\tilde{D}_1$. In this case, decomposing the A_1 sub-band further will not give any improvement and consequently, the reconstructed $\tilde{D}_2$ and $\tilde{D}_3$ sub-bands show less information about the two targets.

4.1 Mean separation

One method to measure the potential of detection improvement is to calculate the mean separation between the interference and the interference with an embedded target. A larger mean separation indicates that the target is more likely to be successfully detected.

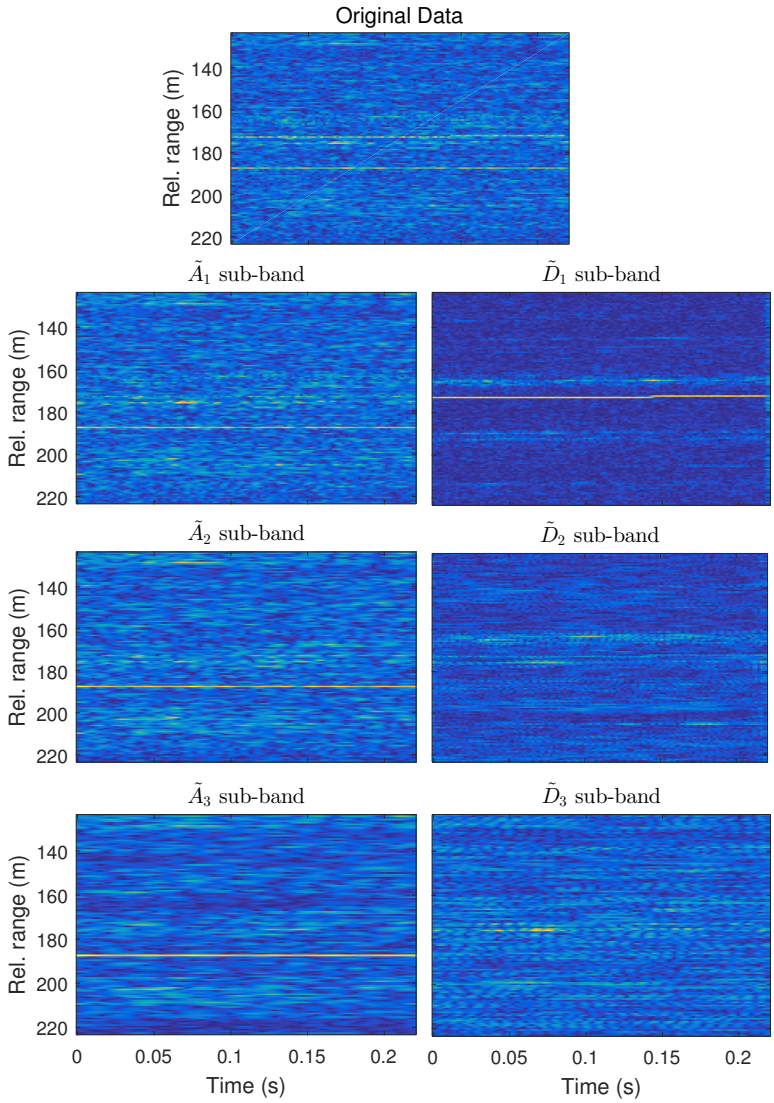

Figure 2: Range / time intensity images with stationary and moving point targets injected into the original data. The stationary target is maintained in the reconstructed $\tilde{A}_k$ sub-band while the moving target is maintained in the first level reconstructed $\tilde{D}_1$ sub-band.

To help visualise this result, the probability density function (PDF) of the data with and without a Swerling 0 target is shown in Fig. 3 for the original HH data, and the reconstructed $\tilde{A}_1$ and $\tilde{D}_1$ sub-bands. Note that for the original data, the PDFs of the stationary and moving target are identical. For the stationary target, $\tilde{A}_1$ shows a reasonable separation between the two distributions while the moving target shows poor separation. These results are reversed for the reconstructed detail sub-band, $\tilde{D}_1$, where there is no separation for the stationary target (the red line sits on top of the blue line) while a large separation is observed for the moving target.

Figure 4 shows the mean separation for a number of reconstructed sub-band combinations using 3 different target radial velocities: 0, 1.1 and 2.6 m/s. These correspond to the centre and edge of the endo-clutter region and the exo-clutter (noise only) region respectively. The mean separations of the original data is shown in blue and represents a reference level for the mean separation analysis. The results for the reconstructed sub-bands are then ranked and shown by a red line with triangles markers.

For the stationary target, the reconstructed sub-band $\tilde{A}_3$ has the biggest mean separation of 5 dB higher than

the unfiltered data followed by $\tilde{A}_2$ and $\tilde{A}_1$. When the target has a radial velocity of 1.1 m/s, the reconstructed combination $\tilde{D}_{23}$ gives the best mean separation of 3 dB, implying that the target Doppler frequency is located between $\tilde{D}_2$ and $\tilde{D}_3$. For a target moving with a radial velocity of 2.6 m/s, the biggest mean separation is shown for the $\tilde{D}_1$ reconstructed sub-band and is 11 dB greater than the original mean separation. In this case, higher levels of SWT do not improve the mean separation as there is little target information in the A_1 sub-band. Note also that the $\tilde{D}_2$ result is quite small while the combination $\tilde{D}_{12}$ is greater than the original mean separation. This is due to the majority of information about the target being maintained in D_1.

After extensive experimentation, a group of reconstructed sub-bands have been selected for further analysis and to test the detection performance. A moving target outside the endo-clutter region will always be present in the $\tilde{D}_1$ reconstructed sub-band while a stationary target will always be located in the $\tilde{A}_1$ reconstructed sub-band. Detecting a slowly moving target is more difficult as it may be present in either the $\tilde{A}_2$ or $\tilde{D}_2$ reconstructed sub-bands or even have a Doppler frequency that lies partway between the frequency extent of these sub-bands. If this happens, it can potentially reduce the detection performance. Therefore to ensure good detection performance in all cases, we have included combinations of $\tilde{D}_1, \tilde{D}_2, \tilde{D}_{12}, \tilde{D}_{23}$ and $\tilde{A}_3$. Unfortunately, the target velocity is not known ahead of time and a method is required to select which sub-band to use to ensure good detection performance.

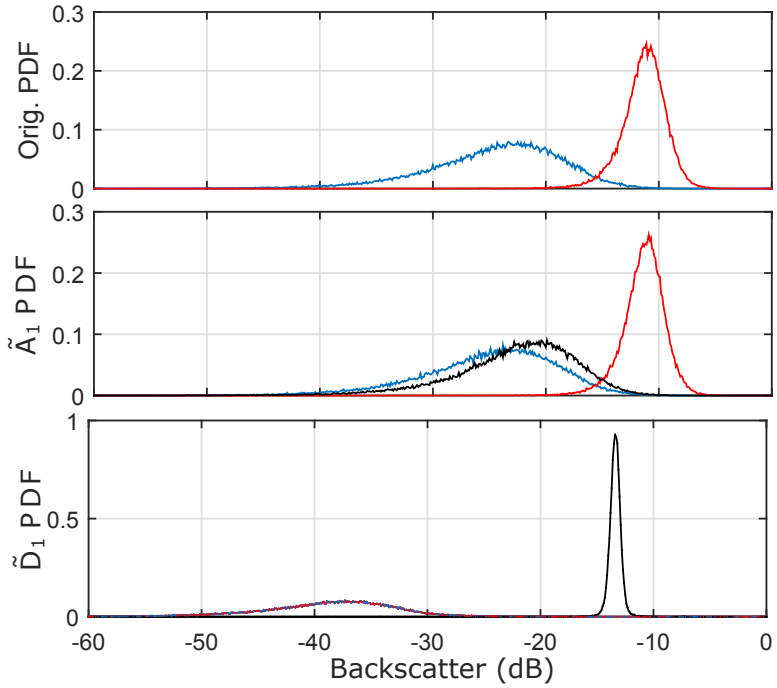

Figure 3: PDFs of the interference only (blue), stationary target plus interference (red) and moving target plus interference (black) for the original data and the $\tilde{A}_1$ and $\tilde{D}_1$ reconstructed sub-bands.

4.2 Entropy

Entropy is a measure of information and has been widely used to measure system disorder in statistical analysis [19]. It is also used to measure the global or average uncertainty of random samples [20, 21]. Entropy has been used to help target detection in sea-clutter via statistic measurement of range spread, feature extraction and measurement of the randomness of the data and target [9–11].

For our study, entropy is proposed as a means of determining which reconstructed sub-band contains the most information about a target and hence would provide the best detection performance. The motivation for

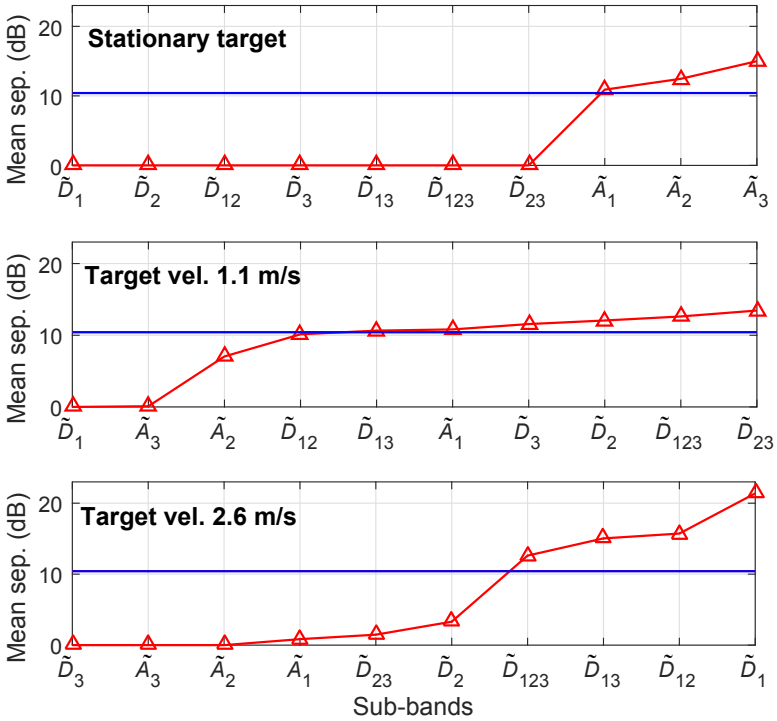

Figure 4: The mean separation for targets having an SIR of 10 dB after SWT processing with sub-band reconstruction. Blue line is the original mean separation and the red is for the reconstructed sub-bands.

using entropy is that the target is persistent over time while the interference returns are more random. The entropy will therefore be different when a target is present.

The entropy of a discrete random variable, X, is given by

$$H(X) = -\sum_{q=1}^{Q} \int_{l_q}^{u_q} g(x_q) \log g(x_q)\, dx_q \tag{6}$$

where $g(x_q)$ is the PDF of the data over Q intervals and the lower and upper limits are l_q and u_q respectively [20]. Let $w_q = u_q - l_q$ be the width of the histogram bin for the q^{th} term in the summation. The bin probabilities can then be written as $p_q = w_q g(x_q)$, giving the final expression for the entropy,

$$H(X) = -\sum_{q=1}^{Q} p_q \log(p_q/w_q), \quad w_q > 0. \tag{7}$$

4.3 Entropy as an indicator

To apply the entropy given in (7), the PDF of the data is determined for each range bin using all the slow-time samples in a given CPI. A smaller entropy value is observed when the distribution has smaller variance and vice versa. To avoid the variation if the entropy of a target is lower or higher than the interference, we define our entropy indicator as the absolute value of the entropy value with zero mean,

$$E(X) = |H(X) - \langle H \rangle|, \tag{8}$$

where $\langle H \rangle$ is the mean entropy over all range bins.

To demonstrate the entropy variation when a target is present, we inject a Swerling 0 target with an SIR of 10 dB into the data using a CPI of 128 pulses and 200 range bins. Figure 5 shows the entropy variation for each range bin using a single level SWT. When the target is stationary (top plot), the $\tilde{A}_1$ reconstructed sub-band produces a peak at the target location while the entropy variations in $\tilde{D}_1$ are small across all range bins. However, when the target moves at a radial velocity of 2.6 m/s (bottom plot), $\tilde{D}_1$ shows a high peak at the target bin and $\tilde{A}_1$ shows little variation. Both of these results match the mean separation observed in Section 4.1.

Figure 6 then shows the entropy metric for a number of reconstructed sub-bands as the SIR increases. Three different target velocities (0, 1.1 and 2.6 m/s) are shown with each result baselined by first determining the maximum entropy over an interference only region and then offsetting the measured entropy value. This ensures that the entropy value for each reconstructed sub-band is equal when no target is present. When the target is stationary, the $\tilde{A}_3$ sub-band has the highest maximum entropy followed by $\tilde{A}_2$ and $\tilde{A}_1$. For the faster moving target, the entropy metric is maximum for the $\tilde{D}_1$ reconstructed sub-band. Lastly, when the target moves at 1.1 m/s, the combination $\tilde{D}_{23}$ reconstructed sub-band is best. Again, these results consistently match the mean separation found in Section 4.1.

Rather than decomposing and isolating every sub-band from our chosen set, we propose a more efficient method where the entropy variations of the sub-bands are compared after each decomposition level. This idea is based on an image processing application for selecting the minimum decomposition level of a natural image [22]. Figure 7 shows the sub-band selection scheme for our detector where the maximum entropy of the reconstructed sub-band X, is $\gamma_X = \max\{E(X)\}$. The first step is to compute the maximum entropy of the $\tilde{A}_1$ and $\tilde{D}_1$ reconstructed sub-bands after a single level of decomposition. If the maximum entropy of $\tilde{D}_1$ is greater than $\tilde{A}_1$, we select $\tilde{D}_1$ to perform the detection because the target is no longer maintained in $\tilde{A}_1$. However, if the maximum entropy of $\tilde{D}_1$ is less than $\tilde{A}_1$, we compute the next level SWT and compare the maximum entropy of $\tilde{D}_2$ and $\tilde{A}_2$. This time, if $\tilde{D}_2$ is larger than $\tilde{A}_2$, we select the maximum of the three reconstructed sub-bands: $\tilde{D}_2, \tilde{D}_{12}$ and $\tilde{D}_{23}$. If $\tilde{A}_2$ has the larger entropy, then a further decomposition to $\tilde{A}_3$ is performed. For most cases, this method reduces the computation cost by avoiding the decomposition and reconstruction of sub-bands which are not necessary.

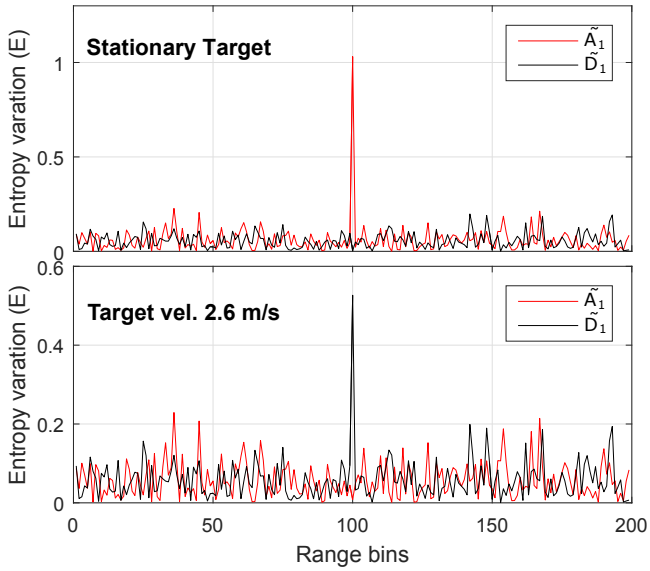

Figure 5: Entropy variation of the data with an injected target at range bin 200: stationary target (top) and moving target with radial velocity 2.6 m/s (bottom). The target has an SIR of 10 dB.

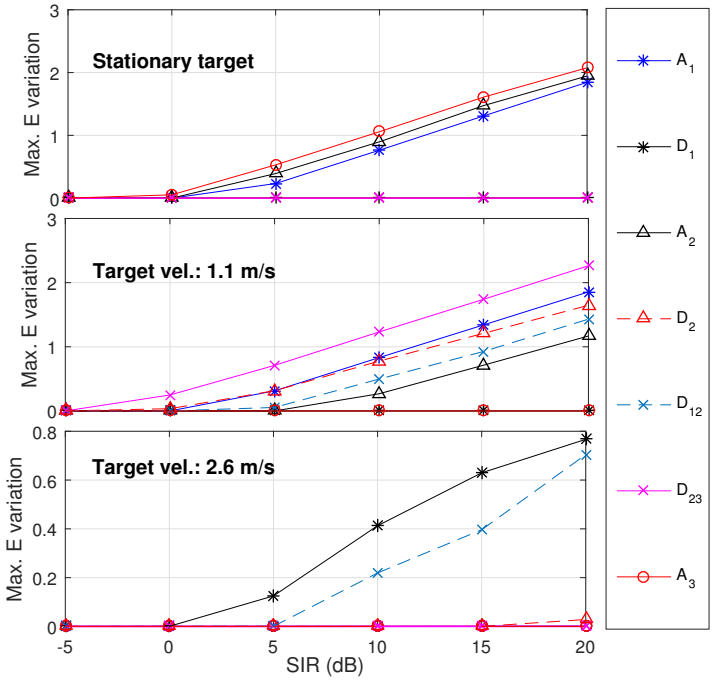

Figure 6: Maximum entropy variation with a Swerling 0 target and increasing SIR.

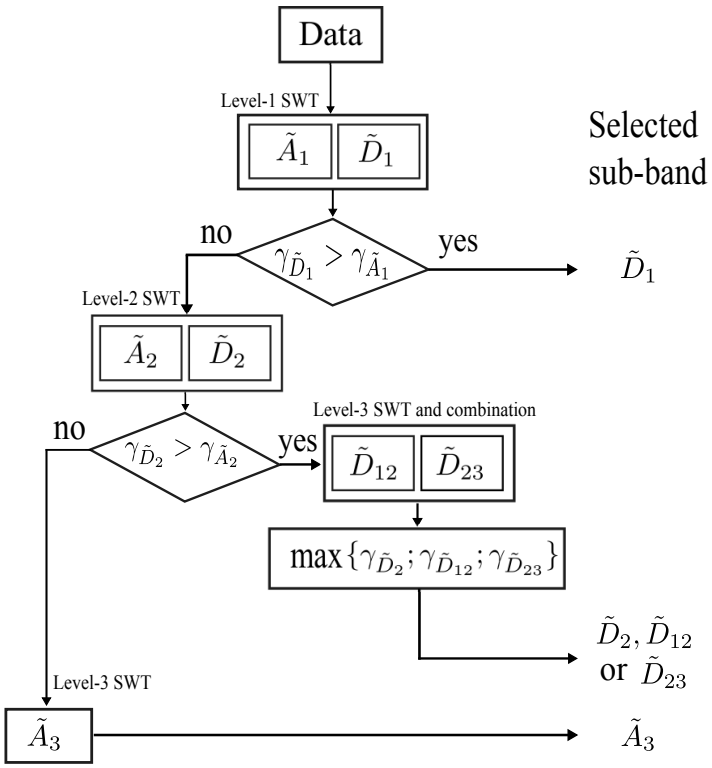

Figure 7: Diagram of entropy sub-band indicator: the entropy of each level SWT sub-band reconstruction are compared. γ is the maximum entropy of each sub-band, used to indicate the sub-band with the most information about the target.

5.0 Detection performance

In this section, we compare the performance of our new detection scheme against unfiltered data in the range / time domain. Variations of the target radial velocity (0, 1.1 and 2.6 m/s) are given with each result also showing the proportion of reconstructed sub-bands. The data used for comparison comprises a CPI of 128 pulses and 200 range bins.

At the output of each detector, the data intensity is input into a CA-CFAR algorithm with the results compared to judge the improvement in SIR for a given probability of detection, P_{d}. It is applied along range to determine a threshold which adapts to the local clutter in order to maintain a desired constant false alarm rate of $P_{\mathrm{fa}} = 10^{-3}$. Monte Carlo simulation is now used to determine the probability of detection by repeatedly injecting point targets at each possible range bin of the data. The target SIR is varied and the detection scheme is run with the adaptive threshold determined by the CA-CFAR algorithm. The probability of detection is then determined by counting the number of detections which cross the threshold.

Three alternative detection cases are now compared. The first uses the unfiltered 'original' data as an input into the CA-CFAR. The second result uses the 'best' SWT reconstructed sub-band as determined by the mean separation analysis in Section 4.1. These comprise $\tilde{A}_3, \tilde{D}_{23}$ and $\tilde{D}_1$ for targets with radial velocities of 0, 1.1 and 2.6 m/s respectively. The third case uses the entropy sub-band indicator to determine which reconstructed sub-band to input into the CA-CFAR. The best performance of this scheme should match the best SWT results.

Figure 8 shows the detection performance (first column) and reconstructed sub-band selections (second column) for a Swerling 0 target using the 3 different target velocities. The non-filtered detection result is shown in blue, while the best reconstructed sub-band detection results are shown in red, magenta and black for the three target velocities. The detection result using the entropy indicator is plotted in dark green and denoted as 'eSWT'. For all the comparisons below, the SIR has been compared at $P_{\mathrm{d}} = 0.5$.

For the stationary target, the detection in the $\tilde{A}_3$ sub-band has the highest detection performance and is about 6 dB over the conventional result. The eSWT performance is not as good as the majority of the indicator results are incorrect when the SIR goes below 5 dB. However it still has a 5 dB improvement over the original result. For the slow moving target, the $\tilde{D}_{23}$ performance is 3 dB above the original, while the eSWT has an improvement of only 2.5 dB. This is because the indicator is often confused between the $\tilde{D}_2$ and $\tilde{D}_{23}$ reconstructed sub-bands. However, since both of these contain information about the target, there is only a minor impact in the final detection result. For the faster moving target, the indicator points to $\tilde{D}_1$ at a rate of almost 100% and the detection result is 7 dB above the original case. Similar results for each target case are also found for a Swerling 1 fluctuating target.

6.0 Conclusion

This paper reported on our application of SWTs to small target detection in sea-clutter. The process of *sub-band isolation and reconstruction* has been proposed to highlight different features of the sea-clutter and better distinguish between targets and sea-spikes. However, selecting the correct sub-band is key for implementing a practical detection scheme when the target's radial velocity is unknown. The first part of the paper therefore quantified the mean separation between the interference and target plus interference of the different reconstructed sub-bands. This study revealed that the stationary target was better detected at low resolutions, while a moving target was better detected at high resolution in the detail sub-band.

Entropy was then proposed as a means of indicating which reconstructed sub-band contains the most information about the target. A computationally efficient scheme was presented based on the maximum entropy at different levels of the SWT decomposition. The last part of the paper then demonstrated the detection performance using a CA-CFAR algorithm. This analysis revealed that without prior knowledge of the target's velocity, the improvement in the required SIR was between 3 and 7 dB when compared to unfiltered data. The

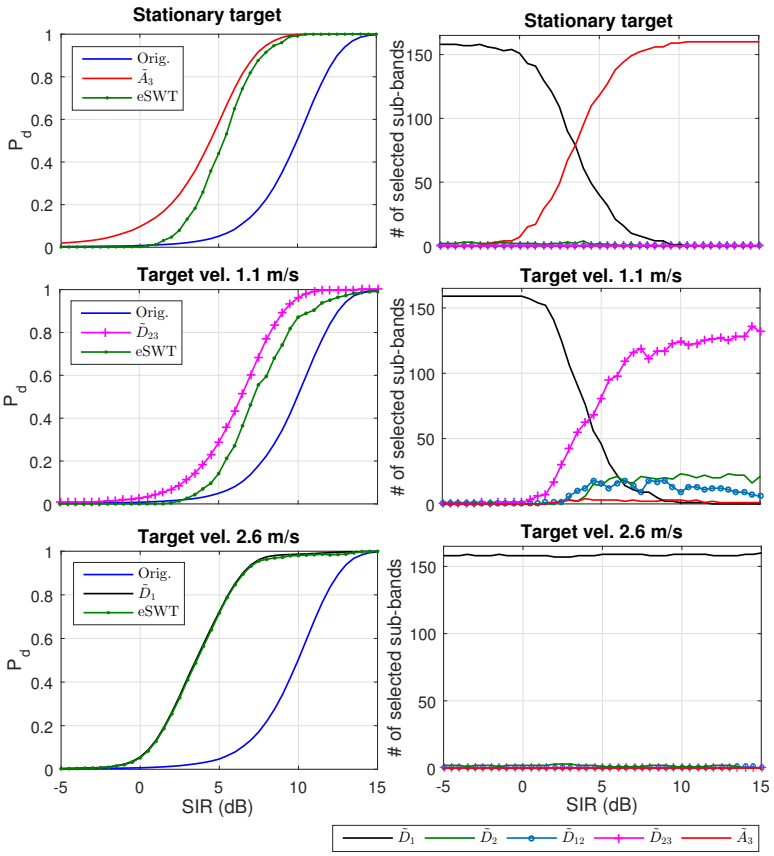

Figure 8: The probability of detection for Swerling 0 target (first column) and the selected reconstructed sub-bands (second column).

entropy indicator was able to successfully determine the 'best' reconstructed sub-band in the majority of cases and also demonstrated a substantial improvement over the unfiltered data.

Future work will investigate the effect of different mother wavelets and look at alternative indication schemes for determining the best choice of reconstructed sub-bands.

References

[1] K. Ward, R. Tough, and S. Watts, *Sea Clutter: Scattering, the K Distribution and Radar Performance*, 2nd ed. Institution of Engineering and Technology, 2013.

[2] M. Long, *Radar reflectivity of land and sea*. Lexington Books, 2001.

[3] L. Rosenberg, "Sea-spike detection in high grazing angle X-band sea-clutter," *IEEE Transactions on Geoscience and Remote Sensing*, vol. 51, no. 8, pp. 4556–4562, 2013.

[4] N. Ehara, I. Sasase, and S. Mori, "Weak radar signal detection based on wavelet transform," in *IEEE International Conference on Acoustics, Speech, and Signal Processing*, vol. 2, Apr 1994, pp. 377–380.

[5] N. Wang, Y. Zhang, and S. Wu, "Radar waveform design and target detection using wavelets," in *CIE International Conference on Radar,*, 2001, pp. 506–509.

[6] S. Zhang, J. Fan, L. Shou, and J. Dong, "A detection method of radar signal by wavelet transforms," in *Fourth International Conference on Fuzzy Systems and Knowledge Discovery*, vol. 2, Aug 2007, pp. 710–714.

[7] G. Davidson and H. Griffiths, "Wavelet detection of low observable targets within sea clutter," in *IEEE International Radar Confererence*, Oct 2002, pp. 238–242.

[8] V. Duk, B. Ng, and L. Rosenberg, "The potential of 2D wavelet transforms for target detection in sea-clutter," in *IEEE Radar Conference*, May 2015, pp. 901–906.

[9] X. Wang, J. Liu, and H. Liu, "Small target detection in sea clutter based on Doppler spectrum features," in *CIE International Conference on Radar*, Oct 2006, pp. 1–4.

[10] R. Guo, M. Hao, M. Li, Y. Ni, and Z. Cheng, "Small targets detection in low resolution sea clutter," in *Asia-Pacific Microwave Conference*, Dec 2008, pp. 1–4.

[11] S. Jia and L. Kong, "A new approach to range spread target detection based on information entropy," in *2nd Asian-Pacific Conference on Synthetic Aperture Radar*, Oct 2009, pp. 560–562.

[12] D. J. Crisp, N. J. Stacy, and A. S. Goh, "Ingara medium-high incidence angle polarimetric sea clutter measurements and analysis," DSTO, Technical Report DSTO-TR-1818, February 2006.

[13] S. Mallat, "A theory for multiresolution signal decomposition: the wavelet representation," *IEEE Transactions on Pattern Analysis and Machine Intelligence*, vol. 11, no. 7, pp. 674–693, Jul 1989.

[14] I. Daubechies, *Ten Lectures on Wavelets*. Philadelphia, PA, USA: Society for Industrial and Applied Mathematics, 1992.

[15] G. P. Nason and B. W. Silverman, "The stationary wavelet transform and some statistical applications," in *Wavelets and Statistics*. Springer-Verlag, 1995, pp. 281–300.

[16] J.-C. Pesquet, H. Krim, H. Carfantan, and J. Proakis, "Estimation of noisy signals using time-invariant wavelet packets," in *Conference Record of The Twenty-Seventh Asilomar Conference on Signals, Systems and Computers*, Nov 1993, pp. 31–34 vol.1.

[17] J. Pesquet, H. Krim, and H. Carfantan, "Time-invariant orthonormal wavelet representations," *IEEE Transactions on Signal Processing*, vol. 44, no. 8, pp. 1964–1970, Aug 1996.

[18] N. Ahuja, S. Lertrattanapanich, and N. Bose, "Properties determining choice of mother wavelet," *IEE Proceedings on Vision, Image and Signal Processing*, vol. 152, no. 5, pp. 659–664, Oct 2005.

[19] C. Shannon, "A mathematical theory of communication," *Bell System Technical Journal*, vol. 27, 1948.

[20] K. F. Wallis, "A note on the calculation of entropy from histograms," *Review Literature And Arts Of The Americas*, October 2006.

[21] B. Harris, "Entropy," *John Wiley and Sons, Inc*, 2006.

[22] M. V. Wickerhauser, *Adapted wavelet analysis from theory to software.*, ser. Ak Peters Series. Taylor & Francis, 1994.